molecules

MDPI

Article

Synthesis, Phase Behavior and Computational Simulations of a Pyridyl-Based Liquid Crystal System

Fowzia S. Alamro [1], Hoda A. Ahmed [2,3,*], Saheed A. Popoola [4] and Asmaa Aboelnaga [5]

[1] Department of Chemistry, College of Science, Princess Nourah Bint Abdulrahman University, Riyadh 11671, Saudi Arabia; fsalamro@pnu.edu.sa
[2] Department of Chemistry, Faculty of Science, Cairo University, Cairo 12613, Egypt
[3] Chemistry Department, College of Sciences, Taibah University, Yanbu 30799, Saudi Arabia
[4] Chemistry Department, Faculty of Science, Islamic University of Madinah, Al-Madinah Al-Munawwarah 42351, Saudi Arabia; abiodun@iu.edu.sa
[5] Department of Chemistry, Faculty of Women for Arts, Science and Education, Ain Shams University, Cairo 11566, Egypt; asmaa_aboelnaga77@yahoo.com
* Correspondence: ahoda@sci.cu.edu.eg

Abstract: A homologous set of liquid crystalline materials (**Tn**) bearing Schiff base/ester linkages were prepared and investigated via experimental and theoretical techniques. Terminal flexible groups of different chain lengths were connected to the end of phenylbenzoate unit while the other end of molecules was attached to the heterocyclic pyridine moiety. The molecular structures of the designed molecules were evaluated by FT-IR, NMR spectroscopic analyses, whereas their mesomorphic properties were investigated by polarized optical microscopy (POM) and differential scanning calorimetry (DSC). They all exhibited dimorphic properties with the exception of the members having the shortest and longest terminal flexible chains (n = 6 and 16), which were monomorphic. The **T16** derivative was further found possessing purely smectic A (SmA) mesophase while others have their lengths covered by nematic (N) phase. Moreover, the computational evaluation of the azomethine derivatives was carried out using a DFT approach. The polarity of the investigated derivatives was predicted to be appreciably sensitive to the size of the system. Furthermore, the Frontier molecular orbitals analysis revealed various distributions of electron clouds at HOMO and LUMO levels.

Keywords: pyridyl based liquid crystals; schiff base/ester; mesophase behavior; computational DFT calculations

Citation: Alamro, F.S.; Ahmed, H.A.; Popoola, S.A.; Aboelnaga, A. Synthesis, Phase Behavior and Computational Simulations of a Pyridyl-Based Liquid Crystal System. *Molecules* **2021**, *26*, 6416. https://doi.org/10.3390/molecules26216416

Academic Editor: Franck Camerel

Received: 28 September 2021
Accepted: 21 October 2021
Published: 24 October 2021

1. Introduction

Today, structure–activity relationship tools have been required to prepare the material in order to achieve proper characteristics for device applications [1–4]. Calamitic LCs are a prominent kind of mesogens that exhibit smectic and N phases due to their anisotropic self-association. As a result, the LC molecular architectures are designed using anisotropic mesogenic shape factors and principles. Several two- or three-ring compounds based on Schiff base/ester LCs have been reported and their optical behaviors were analyzed to obtain the correlation between the geometry of mesogens and their mesophase behaviors [5–9].

Due to their beneficial capacity to impart lateral and/or longitudinal dipoles, together with variations in their molecular geometries, which are reflected in their optical and electrical behaviors, heterocyclic-based LC materials have been of great interest to many researchers [10–24]. Pyridine exhibits a dipole moment of 2.19 D, which is about five-hundredths of that of a cyano group (~4.0 D) [25]; consequently, it influences the stability of the mesophase when it is utilized as a moiety within the mesogens [25–30]. Additionally, the pyridyl moiety is capable of forming intermolecular hydrogen bonding with components that have carboxylic units [31]. The insertion of new mesogenes or heterocyclic rings

and changeable terminal groups will affect the atomic geometry and offer wide mesophase ranges of the resultant materials [32]. Moreover, slight modification within the molecular shape enables new significant changes within the phase transitions and plays an essential role in the kind and stability of the produced phase [33–37].

In order to investigate the structural linearity of synthesized molecules and molecular polarizability, as well as the geometrical parameters of each prepared compound, a DFT approach was used and the results were correlated with the experimental data [33–40]. It is essential to note that the DFT calculations assume a gas phase for all molecules, as such the most favorable predicted geometry could differ from that of empirical which occurs in a condensed phase such as LC mesophase, where more prolonged molecules are usually favored [41].

In this work, we synthesized and investigated the mesomorphic transitional properties of a three-ring homologous series based on Schiff base/ester mesogenic cores. The studied molecules have a heterocyclic pyridine ring in one terminal while the other end is connected to different flexible alkoxy chains. The influence of various alkoxy chains towards the mesomorphic properties of the derivatives was evaluated. Furthermore, important theoretical data were computed via the DFT method for the synthesized molecules and correlated with the experimental results.

2. Experimental

2.1. Synthesis of Materials

Compounds **T6**, **T8**, **T10**, **T12**, **T14** and **T16** were prepared according to Scheme 1:

Details of preparation and spectroscopic characterizations are given in Supplementary Information (Figures S1–S5).

(*E*)-4-((Pyridin-3-ylmethylene)amino)phenyl 4-(hexyloxy)benzoate (**T6**), yield: 90.7%; mp 111.0 °C, FTIR ($\acute{\upsilon}$, cm^{-1}): 2920, 2861 (CH_2 stretching), 1719 (C=O), 1602 (C=N), 1463 (C-O_{Asym}), 1259 (C-O_{Sym}). ^{1}H-NMR (300 MHz, $CDCl_3$): δ = 0.89 (t, 3H, $CH_3(CH_2)_3CH_2CH_2$, J = 7.5 Hz), 1.29–1.46 (m, 6H, $CH_3(CH_2)_3CH_2CH_2$), 1.75 (q, 2H, J = 4.8 Hz, $CH_3(CH_2)_3CH_2CH_2$), 4.07 (t, 2H, $CH_3(CH_2)_3CH_2CH_2$, J = 6.75 Hz), 7.10 (d, 2H, J = 6.6 Hz, Ar-H), 7.32 (d, 2H, J = 6.3 Hz, Ar-H), 7.39 (d, 2H, J = 5.3 Hz, Ar-H), 7.56–7.84 (dd, 1H, py-H), 8.07 (d, 2H, J = 7.5 Hz, Ar-H), 8.32 (d, 1H, J = 6 Hz, py-H), 8.72 (d, 1H, J = 2.1 Hz, py-H), 8.77 (s, 1H, py-H), 9.07 (s, 1H, CH=N). ^{13}C-NMR (125 MHz, DMSO-d_6, $CDCl_3$): δ = 164.74, 163.71, 159.25, 152.48, 150.94, 149.64, 149.05, 135.46, 132.50 (2C), 131.99 (2C), 124.55, 123.21 (2C), 122.59 (2C), 121.22, 115.15, 68.48, 31.44, 28.93, 25.57, 22.53, 14.37. MS (m/z): 402.49, Anal.Calcd for: $C_{25}H_{26}N_2O_3$: Found (Calc.): C, 74.58 (74.60); H, 6.50 (6.51); N, 6.94 (6.96).

(*E*)-4-((Pyridin-3-ylmethylene)amino)phenyl 4-(octyloxy)benzoate (**T8**), yield: 89.0%; mp 78.0 °C, FTIR ($\acute{\upsilon}$, cm^{-1}): 2916, 2869 (CH_2 stretching), 1710 (C=O), 1594 (C=N), 1462 (C-O_{Asym}), 1259 (C-O_{Sym}). ^{1}H-NMR (300 MHz, $CDCl_3$): δ = 0.88 (t, 3H, $CH_3(CH_2)_4CH_2CH_2CH_2$, J = 5.5 Hz), 1.26–1.30 (m, 12H, $CH_3(CH_2)_4CH_2CH_2CH_2$), 1.43 (q, 2H, J = 7.25 Hz, $CH_3(CH_2)_4CH_2CH_2CH_2$), 1.78 (q, 2H, J = 7.25 Hz, $CH_3(CH_2)_4CH_2CH_2CH_2$), 4.06 (t, 2H, $CH_3(CH_2)_4CH_2CH_2CH_2$, J = 6.4 Hz), 7.13 (d, 2H, J = 6.8 Hz, Ar-H), 7.35 (d, 2H, J = 6.6 Hz, Ar-H), 7.41 (d, 2H, J = 5.5 Hz, Ar-H), 7.50–7.54 (dd, 1H, py-H), 8.17 (d, 2H, J = 7.7 Hz, Ar-H), 8.42 (d, 1H, J = 6.2 Hz, py-H), 8.75 (d, 1H, J = 2.8 Hz, py-H), 8.78 (s, 1H, py-H), 9.09 (s, 1H, CH=N). MS (m/z): 430.55, Anal.Calcd for: $C_{27}H_{30}N_2O_3$: Found (Calc.): C, 73.30 (75.32); H, 7.04 (7.02); N, 6.50 (6.51).

(*E*)-4-((Pyridin-3-ylmethylene)amino)phenyl 4-(decyloxy)benzoate (**T10**), yield: 89.0%; mp 79.0 °C, FTIR ($\acute{\upsilon}$, cm^{-1}): 2918, 2871 (CH_2 stretching), 1712 (C=O), 1590 (C=N), 1462 (C-O_{Asym}), 1255 (C-O_{Sym}). ^{1}H-NMR (300 MHz, $CDCl_3$): δ = 0.85 (t, 3H, $CH_3(CH_2)_6CH_2CH_2CH_2$, J = 5.5 Hz), 1.24–1.40 (m, 12H, $CH_3(CH_2)_6CH_2CH_2CH_2$), 1.43 (q, 2H, J = 7.3 Hz, $CH_3(CH_2)_6CH_2CH_2CH_2$), 1.78 (q, 2H, J = 7.3 Hz, $CH_3(CH_2)_6CH_2CH_2CH_2$), 4.10 (t, 2H, $CH_3(CH_2)_6CH_2CH_2CH_2$, J = 6.0 Hz), 7.11 (d, 2H, J = 5.4 Hz, Ar-H), 7.33 (d, 2H, J = 6.3 Hz, Ar-H), 7.40 (d, 2H, J = 5.4 Hz, Ar-H), 7.57 (d, 1H, J = 7.5 Hz, py-H), 8.00 (d, 2H, J = 6.1 Hz, Ar-H), 8.32 (d, 1H, J = 7.5 Hz, py-H), 8.72 (d, 1H, J = 4.1 Hz, py-H), 8.77 (s, 1H, py-H), 9.09 (s, 1H, CH=N).

MS (*m*/*z*): 562.71, Anal.Calcd for: $C_{29}H_{34}N_2O_3$: Found (Calc.): C, 75.97 (75.95); H, 7.45 (7.47); N, 6.09 (6.11).

(*E*)-4-((Pyridin-3-ylmethylene)amino)phenyl 4-(dodecyloxy)benzoate (**T12**), yield: 91.3%; mp 80.0 °C, FTIR ($\acute{v}$, cm^{-1}): 2922, 2873 (CH2 stretching), 1719 (C=O), 1586 (C=N), 1462 (C-OAsym), 1260 (C-OSym). 1H-NMR (300 MHz, CDCl3): δ = 0.86 (t, 3H, $CH_3(CH_2)_8CH_2CH_2CH_2$, *J* = 5.8 Hz), 1.25–1.254 (m, 16H, $CH_3(CH_2)_8CH_2CH_2CH_2$), 1.43 (q, 2H, *J* = 7.1 Hz, $CH_3(CH_2)_8CH_2CH_2CH_2$), 1.76 (q, 2H, *J* = 8.1 Hz, $CH_3(CH_2)_2CH_2CH_8CH_2$), 4.10 (t, 2H, $CH_3(CH_2)_2CH_8CH_2CH_2$, *J* = 6.4 Hz), 7.11 (d, 2H, *J* = 5.6 Hz, Ar-H), 7.33 (d, 2H, *J* = 6.6 Hz, Ar-H), 7.43 (d, 2H, *J* = 5.5 Hz, Ar-H), 7.59 (d, 1H, *J* = 7.7 Hz, py-H), 8.01 (d, 2H, *J* = 6.3 Hz, Ar-H), 8.32 (d, 1H, *J* = 7.6 Hz, py-H), 8.71 (d, 1H, *J* = 4.8 Hz, py-H), 8.77 (s, 1H, py-H), 9.06 (s, 1H, CH=N). MS (*m*/*z*): 590.33, Anal.Calcd for: $C_31H_38N_2O_3$: Found (Calc.): C, 76.50 (76.51); H, 7.77 (7.87); N, 5.78 (5.76).

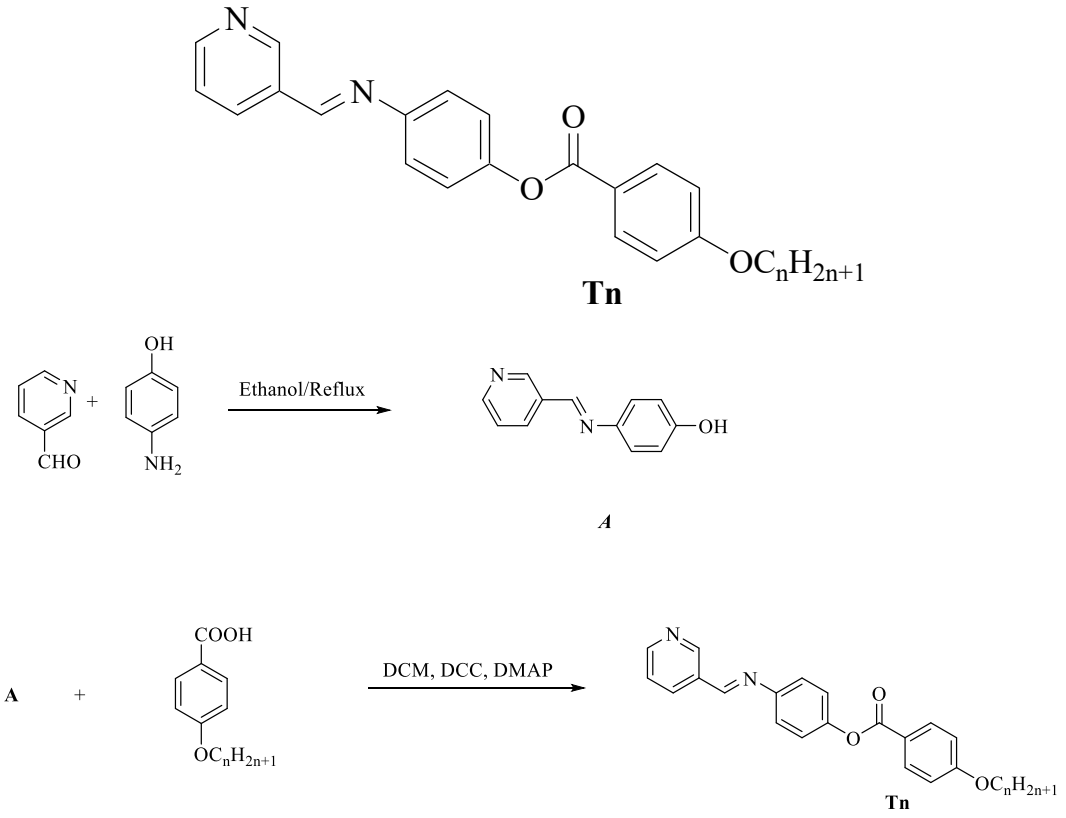

Tn	R
T_6	C_6H_{13}
T_8	C_8H_{17}
T_{10}	$C_{10}H_{21}$
T_{12}	$C_{12}H_{25}$
T_{14}	$C_{14}H_{29}$
T_{16}	$C_{16}H_{33}$

Scheme 1. Synthesis of (*E*)-4-((pyridin-3-ylmethylene)amino)phenyl 4-(alkoxy) benzoate **Tn**. *n* = 6, 8, 10, 12, 14 and 16 carbons.

(*E*)-4-((Pyridin-3-ylmethylene)amino)phenyl 4-(tetradecyloxy)benzoate (**T14**), yield: 92.0%; mp 88.0 °C, FTIR ($\acute{v}$, cm^{-1}): 2922, 2881 (CH_2 stretching), 1717 (C=O), 1595 (C=N), 1466 (C-O_{Asym}), 1259 (C-O_{Sym}). ^{1}H-NMR (300 MHz, $CDCl_3$): δ = 0.86 (t, 3H, $CH_3(CH_2)_{10}CH_2CH_2CH_2$, *J* = 5.6 Hz), 1.25 (m, 20 H, $CH_3(CH_2)_{10}CH_2CH_2CH_2$), 1.43 (q, 2H, *J* = 7.7 Hz, $CH_3(CH_2)_{10}CH_2CH_2CH_2$), 1.74 (q, 2H, *J* = 6.8 Hz, $CH_3(CH_2)_{10}CH_2CH_2CH_2$), 4.11 (t, 2H, $CH_3(CH_2)_{10}CH_2CH_2$

CH_2, *J* = 6.3 Hz), 7.11 (d, 2H, *J* = 5.1 Hz, Ar-H), 7.35 (d, 2H, *J* = 6.0 Hz, Ar-H), 7.39 (d, 2H, *J* = 5.4 Hz, Ar-H), 7.58 (d, 1H, *J* = 7.2 Hz, py-H), 8.06 (d, 2H, *J* = 6.6 Hz, Ar-H), 8.32 (d, 1H, *J* = 7.7 Hz, py-H), 8.71 (d, 1H, *J* = 4.4 Hz, py-H), 8.78 (s, 1H, py-H), 9.08 (s, 1H, CH=N). MS (*m*/*z*): 616036, Anal.Calcd for: $C_{33}H_{42}N_2O_3$: Found (Calc.): C, 77.00 (77.01); H, 8.24 (8.23); N, 5.45 (5.44).

(*E*)-4-((Pyridin-3-ylmethylene)amino)phenyl 4-(hexadecyloxy)benzoate (**T16**), yield: 94.0%; mp 93.0 °C, FTIR ($\acute{v}$, cm^{-1}): 2926, 2879 (CH_2 stretching), 1726 (C=O), 1595 (C=N), 1452 (C-O_{Asym}), 1253 (C-O_{Sym}). ^{1}H-NMR (300 MHz, $CDCl_3$): δ = 0.85 (t, 3H, $CH_3(CH_2)_{12}CH_2CH_2CH_2$, *J* = 5.5 Hz), 1.24–1.40 (m, 24H, $CH_3(CH_2)_6CH_2CH_2CH_2$), 1.67 (q, 2H, *J* = 7.5 Hz, $CH_3(CH_2)_{12}$ $CH_2CH_2CH_2$), 1.75 (q, 2H, *J* = 7.5 Hz, $CH_3(CH_2)_{12}CH_2CH_2CH_2$), 4.07 (t, 2H, $CH_3(CH_2)_{12}CH_2$ CH_2CH_2, *J* = 6.2 Hz), 6.58 (d, 2H, *J* = 5.4 Hz, Ar-H), 6.88 (d, 2H, *J* = 6.3 Hz, Ar-H), 7.07 (d, 2H, *J* = 5.4 Hz, Ar-H), 7.41 (d, 1H, *J* = 7.5 Hz, py-H), 8.24 (d, 1H, *J* = 7.5 Hz, py-H), 8.26 (d, 8.86 (d, 1H, *J* = 4.1 Hz, py-H), 8.87 (s, 1H, py-H), 9.09 (s, 1H, CH=N). MS (*m*/*z*): 646.88, Anal.Calcd for: $C_{35}H_{46}N_2O_3$: Found (Calc.): C, 77.44 (77.45); H, 8.53 (8.54); N, 5.15 (5.16).

2.2. Computational Details

The geometry of the **Tn** compound series studied was fully optimized without geometrical restriction using the GAUSSIAN 09 program (Wallingford, CT 06492 USA) [42]. Frequency calculation was later carried out to establish the convergence nature of the compounds and all the predicted frequencies were found to be real. Furthermore, both Frontier molecular orbitals and the molecular electrostatic potential (MEP) surfaces were generated from the check files (.chk) of optimized molecules. All the calculations were executed using density functional theory (DFT) by employing the B3LYP method [43,44] while utilizing 6–31g(d,p) as the basis set.

3. Results and Discussion

3.1. Mesomorphic Behavior

Representative examples of DSC thermograms for derivatives **T6** and **T14** via both heating and cooling rounds are illustrated in Figure 1. Designed compounds (Figure 1a,b) showed two or three endotherm peaks of transitions during the heating cycle and exothermic transitions during the cooling round, depending on the number and type of formed mesophases according to the corresponding length of the attached terminal alkoxy chain. The POM analysis revealed images which confirmed smectic A and N mesophases (Figure 2) depending on n. The N phase showed threads/a schlieren image and the SmA phase had a focal conic fan texture. The synthesized materials have enantiotropic behavior. Results of the mesomorphic transitions (temperatures, enthalpy and mesophase range) of all the investigated series (**Tn**), as measured from DSC analyses, are collected in Table 1. Moreover, the transition temperatures of all samples were graphically illustrated in Figure 3 in order to investigate the impact of terminal attached flexible chain length on the mesophase property of the series.

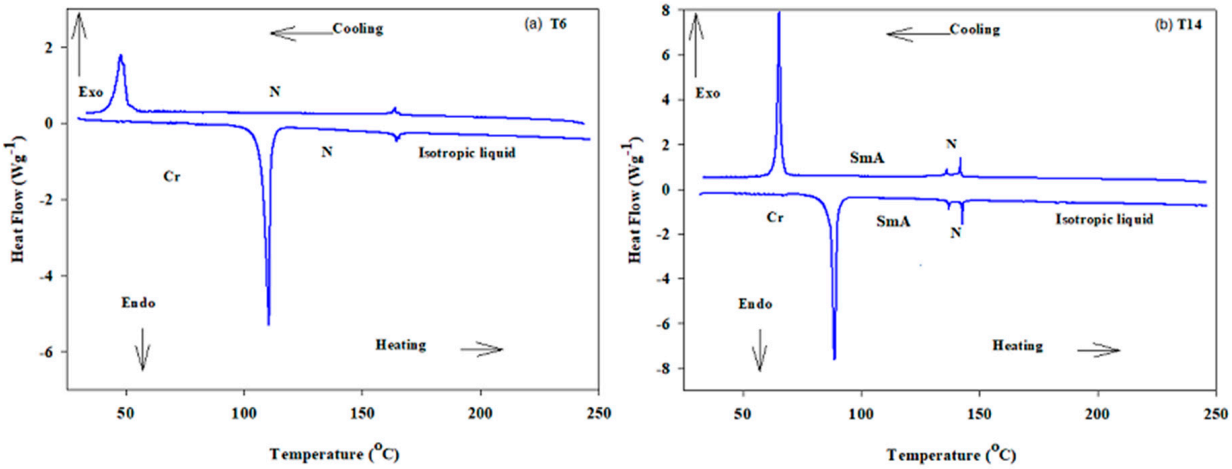

Figure 1. DSC thermograms of (**a**) **T6** and (**b**) **T14** samples.

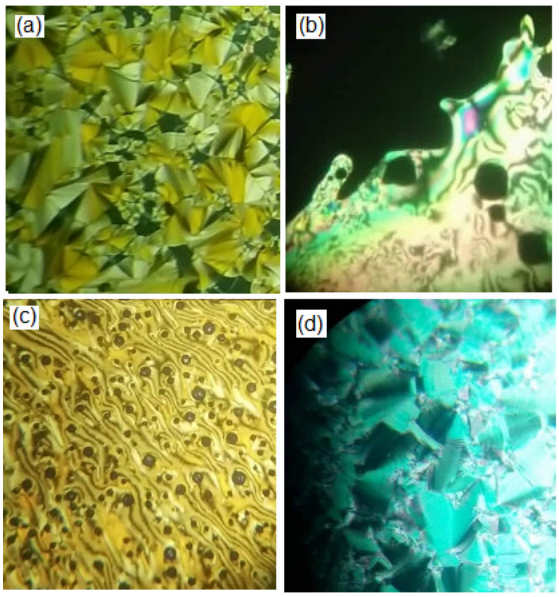

Figure 2. POM textures via heating of (**a**) SmA phase at 102 °C for **T14** derivative; (**b**) N phase at 150 °C for **T14** derivative; (**c**) N phase at 130 °C for **T6** derivative and (**d**) SmA phase at 110 °C for **T16** derivative.

Table 1. Phase transition temperatures (°C) and (enthalpy of transitions in kJ/mol) of **Tn**.

Compounds	$T_{Cr\text{-}SmA}$	$T_{Cr\text{-}N}$	$T_{SmA\text{-}N}$	$T_{SmA\text{-}I}$	$T_{N\text{-}I}$	$\Delta T_{SmA\text{-}N}$	ΔT_{SmA}	ΔT_{N}
T6		110.5 (40.56)	-	-	164.4 (1.46)	-	-	53.9
T8	77.8 (34.43)	-	101.6 (1.55)	-	153.1 (1.23)	23.8	-	51.5
T10	79.3 (37.03)	-	118.9 (1.43)	-	149.7 (1.31)	39.6	-	30.8
T12	80.4 (55.4)	-	131.2 (1.91)	-	153.1 (1.44)	50.8	-	21.9
T14	88.9 (53.22)	-	137.2 (2.18)	-	142.9 (1.74)	48.3	-	5.7
T16	92.9 (57.51)	-	-	139.5 (2.07)	-	-	46.6	-

Cr-SmA = crystal to the SmA mesophase; Cr-N = crystal to the N mesophase; SmA-N = SmA to the N mesophase; SmA-I = SmA to the isotropic mesophase; N-I = nematic to the isotropic mesophase.

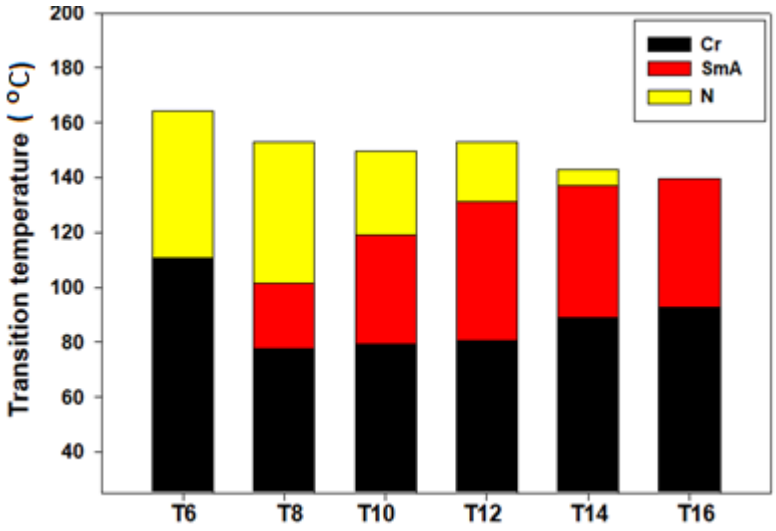

Figure 3. Effect of terminal length on the mesomorphic behavior of **Tn** series.

The results presented in Table 1 and Figure 3 revealed that the melting transitions have an irregular manner with the increasing number of carbons in the terminal chain (n = 6 to 16). Melting temperatures are related to the polarizability and molecular shape of the designed compounds [45]. Moreover, all the compounds of the group (**Tn**) are enantiotropic with a high good mesomorphic range and thermal stability. For the shortest chain derivative (**T6**), it has a monomorphic property exhibiting purely nematogenic phase. The N mesophase stability and range for **T6** are 164.4 and 53.9 °C, respectively. By lengthening the terminal alkoxy chain from n = 6 to 8, the SmA starts to appear and the N phase stability decreases to 153.1 °C together with the N range, which descends to 51.5 °C for **T8**. Compounds **T10**, **T12** and **T14** are also found to be dimorphic, exhibiting SmA and N mesophases. The SmA range and stability increases with the increasing terminal length of flexible chain n from 8 to 14 carbons, but the reverse is the case for the N phase thermal stability and range (Table 1). The resultant phase becomes purely smectogeic in the compound with the longest chain in the series (**T16**). Data suggest that **T16** derivative possesses only a monomorphic SmA mesophase with thermal stability and range of 139.5 and 46.6 °C, respectively. In general, the stability of the N phase decreases while the SmA phase increases with increasing terminal chain length [46,47]. The reduction trend in the N phase thermal transition may be due to the rigid mesogen dilution. Nevertheless, the production of SmA phase reduced the nematogenic range as the alkoxy chain length increases. This could be attributed to the increment of the van der Waals forces of attraction within the long terminal chains that facilitated the lamellar packing for the appearance of the smectic phase.

The normalized entropy changes ($\Delta S/R$) of the produced mesophases were estimated for all samples and summarized in Table 2. This was found to be independent of the size of the system as random trend and little magnitudes of the $\Delta S/R$ related to the SmA-N, N-I transitions were observed. However, the observed little values in all materials can be due to some degree of biaxiality formed by the ester group, which in return decreases the SmA-N, N-I entropy changes [48–50]. The alteration in the entropy changes with alkoxy terminal chains may be ascribed to the interactions between molecules, which are influenced by dipole moment, polarizability, inflexibility, length/breadth proportion and the structural shape of the molecules. These structural parameters may contribute to the conformational, translational and orientational entropies of the molecule in different magnitudes. In spite of the fact that the increment of alkoxy chain length has dilution impact of core/core interactions, it raises the polarizability of the whole molecule, which in return increases the intermolecular strengths between adjoining molecules that advances the degree of molecular ordering. The increment of $\Delta S/R$ values with the expansion

of the carbon numbers in a flexible chain is likely due to the diminishing of the long orientational arrangement and the increment of the conformational number dispersions at the mesophase transitions.

Table 2. Normalized entropy changes of transitions for present series **Tn**.

Compounds	$\Delta S_{SmA-N}/R$	$\Delta S_{SmA-I}/R$	$\Delta S_{N-I}/R$
T6	-	-	0.40
T8	0.50	-	0.35
T10	0.44	-	0.37
T12	0.57	-	0.41
T14	0.64	-	0.49
T16	-	0.6	-

3.2. Computational DFT Calculations and Geometrical Parameters

3.2.1. Reactivity Parameters

The reactivity of chemical compounds is usually inferred from the HOMO–LUMO energy gap (ΔE) together with the ionization potential (I.P) and electron affinity (EA) [51,52]. Following the optimization calculation, the reactivity parameters highlighted in Table 3 were computed for the Tn series. The result shows similar chemical reactivity for all the derivatives as the same values were predicted for the corresponding reactivity indicators. This suggests that the size of the system does not play a significant role in the reactivity of the series. However, the polarity of the derivatives seems to be a bit sensitive to the size of the system as the calculated dipole moment listed in Table 3 and the dipole moment vectors (x and z directions) portrayed in Figure S6 gradually increased with the increasing alkoxy chain length. Regarding the Frontier molecular orbital depicted in Figure 4, the similar HOMO and LUMO distributions recorded for the all the derivatives could be attributed to the nearly equal corresponding HOMO and LUMO energy levels highlighted in Table 3 [52]. On the part of HOMO, the electron clouds were predicted to be evenly allocated over the carbon atoms and the π-electrons system of the pyridyl ring and its immediate phenyl as well as their C=N linkage. Moreover, an appreciable cloud distribution was recorded over the second phenyl ring carbon and its π-electrons together with the alkoxy oxygen. On the other hand, the second phenyl ring and the alkoxy oxygen at the LUMO level were found to be electron deficient while electron clouds distribution only covered the carbon atoms of the pyridyl and the first phenyl rings as well as their C=N linkage. On the part of the molecular electrostatic potential (MEP) presented in the Figure 5, the carbonyl oxygen of the ester linkage in each of the **Tn** series has high electron density but low electrostatic potential as reflected by the red cloud over its region [53–55]. Similarly, an appreciable electron density was observed for the pyridyl nitrogen heteroatom, C=N linkage nitrogen atom and alkoxyl oxygen of the derivatives. It could be concluded that the kind and the thermal stability of the formed phases facilitate the molecular space-filling due to the attached terminals that influence the physical geometrical parameters to enhance the intermolecular attractions between molecules. Moreover, the high electron density predicted for the carbonyl oxygen of –OCO- linkage together with the appreciable quantity recorded for that of -C=N- linkage, as reflected in Figure 5, suggests significant contribution of these linkages to the derivatives' polarizability, which is an important factor that increases the mesophase thermal stability of a compound [56,57].

Table 3. Reactivity and polarity parameters of the **Tn** series calculated at the B3LYP/6–31g(d,p) level.

Compound	E_{HOMO} (eV)	E_{LUMO} (eV)	ΔE (eV)	Dipole Moment (Debye)	I.P (eV)	E.A (eV)	Polarizability ($Bohr^3$)
T6	−5.8926	−1.8294	4.0632	4.2156	5.8926	1.8294	333.3200
T8	−5.8902	−1.8286	4.0616	4.2622	5.8902	1.8286	356.7500
T10	−5.8894	−1.8283	4.0610	4.2873	5.8894	1.8283	379.8900
T12	−5.8891	−1.8281	4.0610	4.3020	5.8891	1.8281	402.9000
T14	−5.8888	−1.8281	4.0608	4.3110	5.8888	1.8281	425.8300
T16	−5.8885	−1.8278	4.0608	4.3170	5.8885	1.8278	448.7200

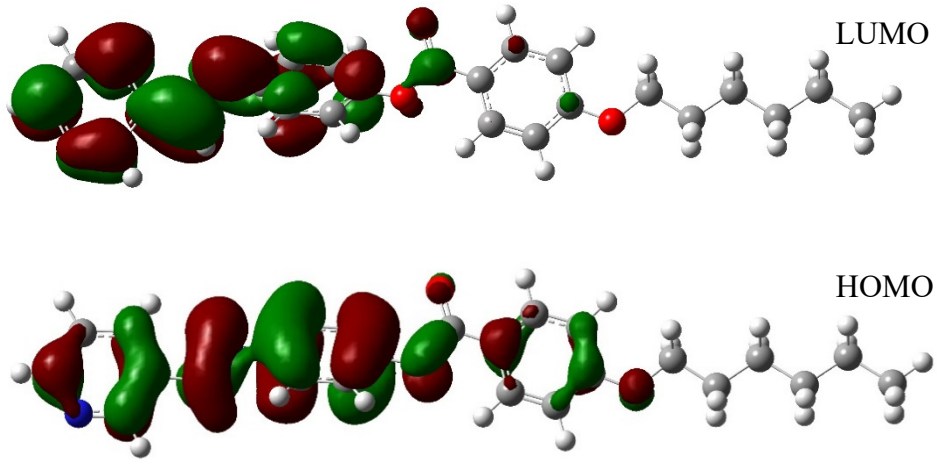

T6

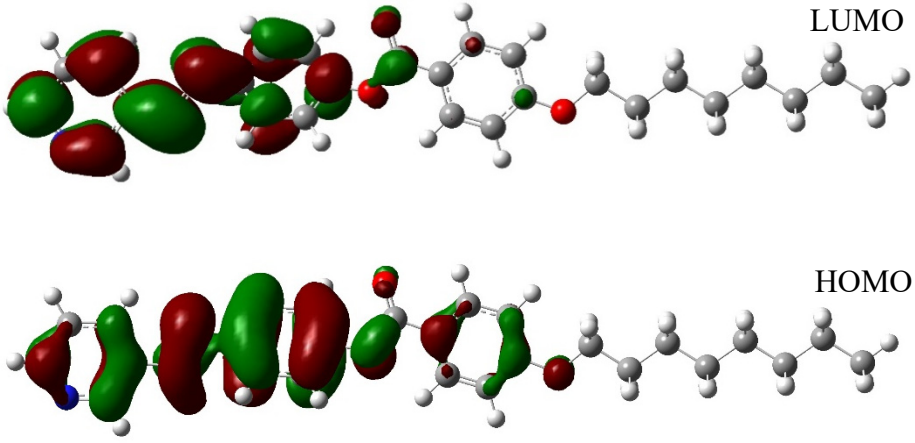

T8

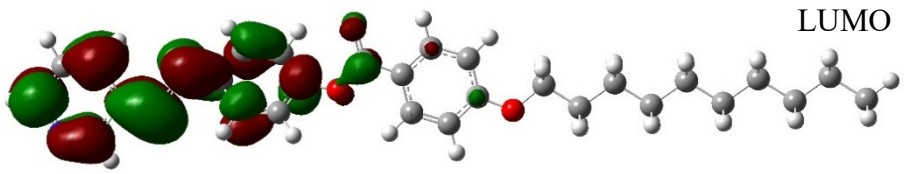

Figure 4. *Cont.*

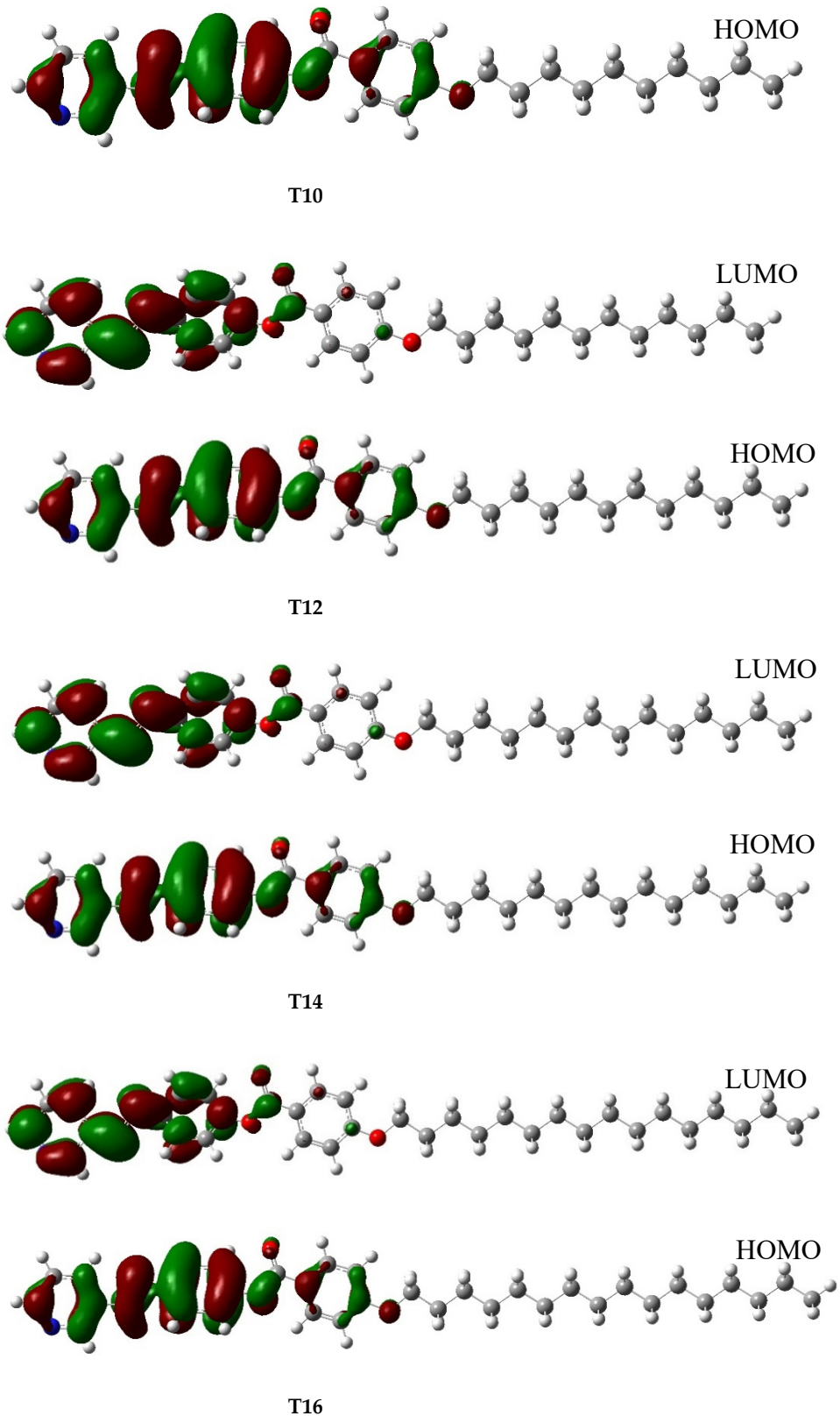

Figure 4. Frontier molecular orbitals for the compound **Tn** calculated at the B3LYP/6–31g(d,p) level.

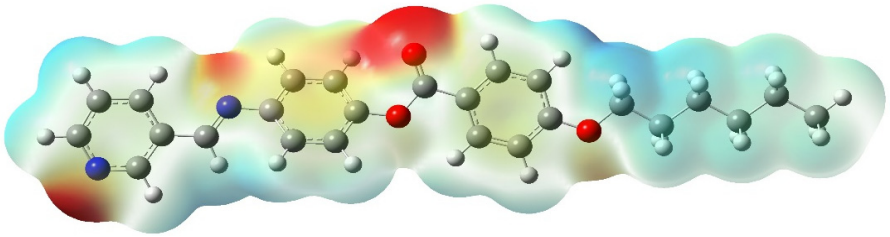

T6

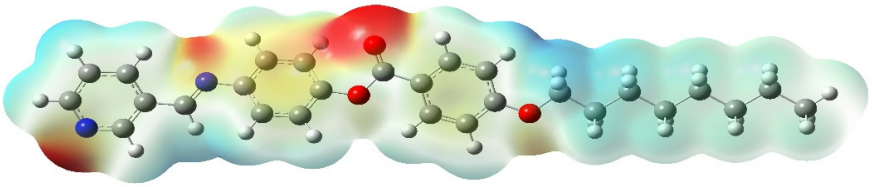

T8

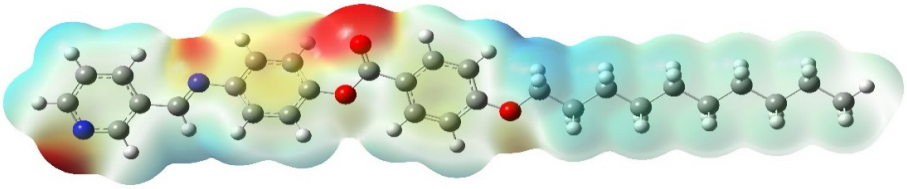

T10

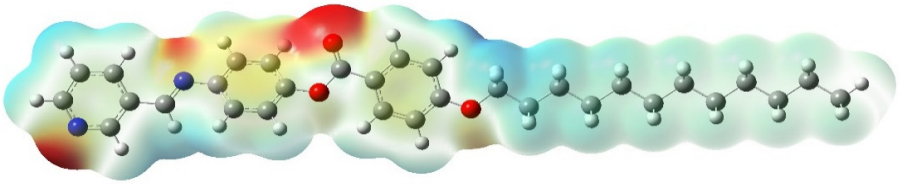

T12

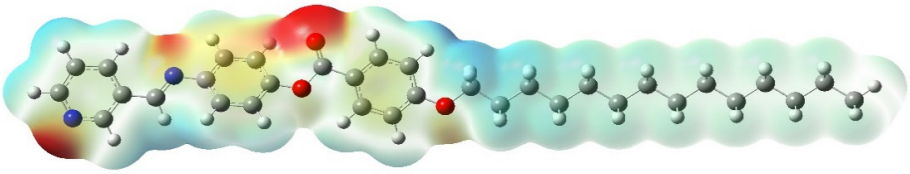

T14

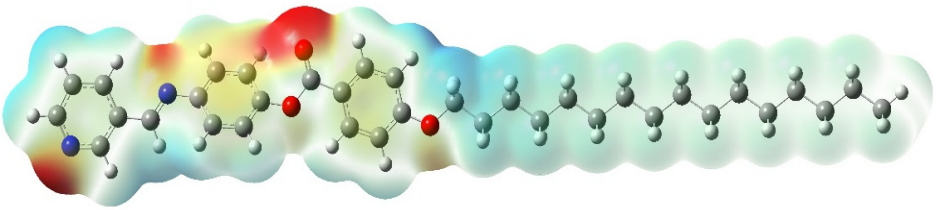

T16

Figure 5. Molecular electrostatic potential (MEP) recorded at an isovalue of 0.001 and calculated at the B3LYP/6–31g(d,p) level for the **Tn** series.

3.2.2. Energy

The calculated zero-point energy and thermal energy, as well as the thermodynamic parameters listed in Table 4, were calculated to increase with the size of the derivative in the series. This result quite agrees with reports in the literature as the energy is an extensive property [54,55]. According to McMillan relation [58,59] the enthalpy change associated with the Smectic to nematic transition (Table 1) increases as the width of the N phase reduces. Theoretically, the predicted enthalpy changes for molecules increase with the terminal chain length (n). Furthermore, the calculated thermal energy accents to the thermal stability highlighted for the SmA-N transition of the derivatives in Table 1 were recorded to increase with size of the system. In the same vein, the predicted entropy is consistent with the normalized entropy (Table 2) obtained for the **Tn** series.

Table 4. Zero-point energy, thermal energy and thermodynamic parameters in kcalmol^{-1} for the compound **Tn** series calculated at the B3LYP/6–31g(d,p) level.

Compound	ZPE	Thermal	Enthalpy	Gibbs	Entropy
T6	289.4371	307.0444	307.6374	248.3823	198.7430
T8	325.2554	344.5532	345.1456	281.8461	212.3080
T10	361.0542	382.0526	382.6449	315.1104	226.5120
T12	396.8505	419.5507	420.1430	348.3339	240.8490
T14	432.6443	457.0482	457.6405	381.5380	255.2480
T16	468.4387	494.5450	495.1380	414.7377	269.6630

4. Conclusions

New mesomorphic pyridyl series' with -CH=N- and -OCO- connecting linkages, *(E)-4-((pyridin-3-ylmethylene)amino)phenyl 4-(alkoxy) benzoate*, were synthesized and experimentally as well as theoretically investigated. Molecular structures were elucidated using elemental analyses, FT-IR and ^{1}H-NMR spectroscopy. Liquid crystalline activities of prepared derivatives were examined by DSC and POM analyses. Theoretical simulations were carried out by DFT calculation method.

The study revealed that:

- All designed heterocyclic compounds exhibit good thermal mesomorphic stability with enantiotropic transitions.
- The N mesophase covers all lengths of the series except the longest chain member (n = 16) exhibiting purely a smectogenic phase.
- Geometrical simulation parameters of the formed derivatives are highly affected by the mesomeric nature of the pyridyl moiety and the terminal extremes of alkoxy chains.
- The polarity and polarizability of the investigated derivatives seem to be a bit sensitive to the length of the designed system.
- The Frontier molecular orbital analysis shows even distribution of electron clouds over the carbon atoms and the π-electrons system of the pyridyl and phenyl rings together with C=N linkage at both HOMO and LUMO levels.
- The MEP affirm the carbonyl oxygen of the ester linkage to be of high electron density but low electrostatic potential.
- The calculated thermal energy accents to the experimental values of thermal stability were recorded to increase with size of the system.

Supplementary Materials: The following are available online: Figure S1: ^{1}H-NMR spectrum of **T6**; Figure S2: ^{13}C-NMR spectrum of **T6**; Figure S3: ^{1}H-NMR spectrum of **T10**; Figure S4: ^{1}H-NMR spectrum of **T12**; Figure S5: ^{1}H-NMR spectrum of **T14**; Figure S6: Atomic charges and dipole moment vectors, calculated at B3LYP/6–31G(d,p) level for the **Tn** series.

Author Contributions: Formal analysis, A.A., H.A.A., and F.S.A.; Funding acquisition, F.S.A. and H.A.A.; Methodology, F.S.A.,A.A., S.A.P. and H.A.A.; Project administration, F.S.A. and H.A.A.; Resources and Software, S.A.P. and H.A.A.; Writing—original draft, H.A.A., S.A.P., F.S.A. and A.A.; Writing—review and editing, H.A.A. and S.A.P. All authors have read and agreed to the published version of the manuscript.

Funding: This research received no external funding.

Institutional Review Board Statement: Not applicable.

Informed Consent Statement: Not applicable.

Data Availability Statement: The data presented in this study are available on request from the corresponding author.

Conflicts of Interest: The authors declare no conflict of interest.

Sample Availability: Samples of the compounds are available from the authors.

References

1. Imrie, C.T.; Henderson, P.A.; Yeap, G.Y. Liquid crystal oligomers: Going beyond dimers. *Liq. Cryst.* **2009**, *36*, 755–777. [CrossRef]
2. Yeap, G.Y.; Lee, H.C.; Mahmood, W.A.K.; Imrie, C.T.; Takeuchi, D.; Osakada, K. Synthesis, thermal and optical behaviour of non-symmetric liquid crystal dimers α-(4-benzylidene-substituted-aniline-4′-oxy)-ω-[pentyl-4-(4′-phenyl) benzoateoxy] hexane. *Phase Transit.* **2011**, *84*, 29–37. [CrossRef]
3. Yeap, G.Y.; Osman, F.; Imrie, C.T. Non-symmetric dimers: Effects of varying the mesogenic linking unit and terminal substituent. *Liq. Cryst.* **2015**, *42*, 543–554. [CrossRef]
4. Yeap, G.Y.; Hng, T.C.; Yeap, S.Y.; Gorecka, E.; Ito, M.M.; Ueno, K.; Okamoto, M.; Mahmood, W.A.K.; Imrie, C.T. Why do non-symmetric dimers intercalate? The synthesis and characterisation of the α-(4-benzylidene-substituted-aniline-4′-oxy)-ω-(2-methylbutyl-4′-(4″-phenyl) benzoateoxy) alkanes. *Liq. Cryst.* **2009**, *36*, 1431–1441. [CrossRef]
5. Maximean, D.M.; Danila, O.; Ganea, C.P.; Almeida, P.L. Filling in the voids of electrospun hydroxypropyl cellulose network: Dielectric investigations. *Eur. Phys. J. Plus* **2018**, *133*, 1–7. [CrossRef]
6. Chiriac, F.L.; Iliş, M.; Madalan, A.; Manaila-Maximean, D.; Secu, M.; Cîrcu, V. Thermal and emission properties of a series of Lanthanides Complexes with N-Biphenyl-Alkylated-4-Pyridone Ligands: Crystal structure of a Terbium complex with N-Benzyl-4-Pyridone. *Molecules* **2021**, *26*, 2017. [CrossRef]
7. Segura, J.L.; Mancheño, M.J.; Zamora, F. Covalent organic frameworks based on Schiff-base chemistry: Synthesis, properties and potential applications. *Chem. Soc. Rev.* **2016**, *45*, 5635–5671. [CrossRef] [PubMed]
8. Gowda, A.; Jacob, L.; Joy, N.; Philip, R.; Pratibha, R.; Kumar, S. Thermal and nonlinear optical studies of newly synthesized EDOT based bent-core and hockey-stick like liquid crystals. *New J. Chem.* **2018**, *42*, 2047–2057. [CrossRef]
9. Matsunaga, Y.; Akagawa, R.; Satou, K.; Uchida, T.; Yamamoto, K. Mesomorphic properties of 3-pyridyl 4-(4-alkoxybenzyleneamino) benzoates and isomeric compounds. *Mol. Cryst. Liq. Cryst. Sci. Technol. Sect. A Mol. Cryst. Liq. Cryst.* **2000**, *350*, 177–186. [CrossRef]
10. Campbell, N.L.; Duffy, W.L.; Thomas, G.I.; Wild, J.H.; Kelly, S.M.; Bartle, K.; O'Neill, M.; Minter, V.; Tuffin, R.P. Nematic 2,5disubstituted thiophenes. *J. Mater. Chem.* **2002**, *12*, 2706–2721. [CrossRef]
11. Parra, M.; Elgueta, E.; Ulloa, J.; Vergara, J.; Sánchez, A. Columnar liquid crystals based on amino-1,3,4-thiadiazole derivatives. *Liq. Cryst.* **2012**, *39*, 917–925.
12. Seltmann, J.; Lehmann, M. Low-melting nematic V-shaped1,3,4-thiadiazoles—Phase engineering using small substituents and mixtures of flexible chains. *Liq. Cryst.* **2011**, *38*, 407–422. [CrossRef]
13. Ester, D.F.; Mckearney, D.; Herasymchuk, K.; Williams, V.E. Heterocycle effects on the liquid crystallinity of terthiophene analogues. *Materials* **2019**, *12*, 2314. [CrossRef] [PubMed]
14. Alamro, F.S.; Gomha, S.M.; Shaban, M.; Altowyan, A.S.; Abolibda, T.Z.; Ahmed, H.A. Optical investigations and photoactive solar energy applications of new synthesized Schiff base liquid crystal derivatives. *Sci. Rep.* **2021**, *11*, 6233.
15. Han, J.; Wang, J.; Zhang, F.; Zhu, L.; Pang, M.; Meng, J. Synthesis and mesomorphic behaviour of heterocycle-based liquid crystals containing 1,3,4 oxadiazole/thiadiazole and thiophene units. *Liq. Cryst.* **2008**, *35*, 1205–1214. [CrossRef]
16. Dos Santos, D.R.; Silva de Oliveira, A.G.; Coelho, R.L.; Begnini, I.M.; Magnago, R.F.; Da Silvac, L. Synthesis of liquid crystals materials derived from oxadiazole, isoxazole and tetrazole heterocycles. *Arkivoc* **2008**, *2008*, 157–166. [CrossRef]
17. Shanker, G.; Tschierske, C. Synthesis of non-symmetrically substituted 1,2,4-oxadiazole derived liquid crystals. *Tetrahedron* **2011**, *67*, 8635–8638. [CrossRef]
18. Alamro, F.S.; Ahmed, H.A.; Mostafa, A.M.; Naoum, M.M. Thermal and Mesomorphic Investigations of 1: 1 Supramolecular Assemblies of 4-[(4-(n-Alkoxy) phenylimino) methyl] benzoic Acids Having Symmetrical and Un-Symmetrical Terminal Chain Lengths. *Symmetry* **2021**, *13*, 1785. [CrossRef]
19. Rahman, L.; Hegde, G.; Yusoff, M.M.; Malek, M.N.F.A.; Srinivasa, H.T.; Kumar, S. New pyrimidine-based photo-switchable bent-core liquid crystals. *New J. Chem.* **2013**, *37*, 2460–2467.

20. Thompson, M.; Carkner, C.; Bailey, A.; Mosey, N.J.; Kapernaum, N.; Lemieux, R.P. Tuning the mesogenic properties of 5-alkoxy-2-(4-alkoxyphenyl) pyrimidine liquid crystals: The effect of a phenoxy end-group in two sterically equivalent series. *Liq. Cryst.* **2014**, *41*, 1246–1260. [CrossRef]
21. Devadiga, D.; Ahipa, T.N. Recent synthetic advances in pyridine-based thermotropic mesogens. *RSC Adv.* **2019**, *9*, 23161–23228. [CrossRef]
22. Ong, L.-K.; Ha, S.-T.; Yeap, G.-Y.; Lin, H.-C. Heterocyclic pyridine-based liquid crystals: Synthesis and mesomorphic properties. *Liq. Cryst.* **2018**, *45*, 1574–1584. [CrossRef]
23. Vardar, D.; Kılıç, H.A.; Ocak, H.; Jeannin, O.; Camerel, F.; Eran, B.B. Pyridine-based chiral smectogens: Effects of polar end groups on liquid crystal properties. *Liq. Cryst.* **2021**, *48*, 616–625. [CrossRef]
24. Hagar, M.; Ahmed, H.A.; Alhaddad, O.A. Experimental and theoretical approaches of molecular geometry and mesophase behaviour relationship of laterally substituted azopyridines. *Liq. Cryst.* **2019**, *46*, 1440–1451. [CrossRef]
25. Nelson, J.R.D.; Lide, D.R.; Maryott, A.A. Selected values of electric dipole moments for molecules in the gas phase. In *CRC Handbook of Chemistry and Physics*, 65th ed.; Weast, R.C., Ed.; CRC Press, Inc.: Boca Raton, FL, USA, 1984–1985; pp. E58–E60.
26. Nash, J.A.; Gray, G.W. Studies of some heterocyclic mesogens. *Mol. Cryst. Liq. Cryst.* **1974**, *25*, 299–321. [CrossRef]
27. Burrow, M.P.; Gray, G.W.; Lacey, K.J. The synthesis and liquid crystal properties of some 2,5-disubstituted pyridines. *Liq. Cryst.* **1988**, *3*, 1643–1653. [CrossRef]
28. Karamysheva, L.A.; Kovshev, E.I.; Pavluchenko, A.I.; Roitman, K.V.; Titov, V.V.; Torgova, S.I.; Grebenkin, M.F. New heterocyclic liquid crystalline compounds. *Mol. Cryst. Liq. Cryst.* **1981**, *67*, 241–252. [CrossRef]
29. Petrov, V.F.; Pavluchenko, A.I.; Smirnova, N.I. New liquid crystalline pyridine derivatives. *Mol. Cryst. Liq. Cryst.* **1995**, *265*, 47–53. [CrossRef]
30. Kelly, S.M.; Novel, F.J. 2-(4-octylphenyl)pyridine-5-yl alkanoates and alkenoates: Influence of dipoles and chain conformation on smectic c formation. *Liq. Cryst.* **1996**, *20*, 77–93. [CrossRef]
31. Liu, Z.; Han, J.; Zhang, J.; Yu, Z.; Li, T.; Zhang, S. Synthesis and mesomorphic properties of new fluorinated hydrogen-bonded supramolecular liquid crystals. *Mon. Chem.* **2014**, *145*, 71–77. [CrossRef]
32. Gulbas, H.; Coskun, D.; Gursel, Y.; Bilgin-Eran, B. Synthesis, characterization and mesomorphic properties of side chain liquid crystalline oligomer having schiff base type mesogenic group. *Adv. Mater.* **2014**, *5*, 333–338. [CrossRef]
33. Al-Mutabagani, L.A.; Alshabanah, L.A.; Ahmed, H.A.; Alalawy, H.H. Synthesis, Mesomorphic and Computational Characterizations of Nematogenic Schiff Base Derivatives in Pure and Mixed State. *Molecules* **2021**, *26*, 2038. [CrossRef] [PubMed]
34. Ahmed, H.A.; AEl-Atawy, M. Synthesis, mesomorphic and geometrical approaches of new non-symmetrical system based on central naphthalene moiety. *Liq. Cryst.* **2021**, *48*, 1–13. [CrossRef]
35. El-Atawy, M.A.; Alhaddad, O.A.; Ahmed, H.A. Experimental and geometrical structure characterizations of new synthesized laterally fluorinated nematogenic system. *Liq. Cryst.* **2021**, *48*, 1–11. [CrossRef]
36. Al-Zahrani, S.A.; Ahmed, H.A.; El-Atawy, M.A.; Abu Al-Ola, K.A.; Omar, A.Z. Synthetic, Mesomorphic, and DFT Investigations of New Nematogenic Polar Naphthyl Benzoate Ester Derivatives. *Materials* **2021**, *14*, 2587. [CrossRef] [PubMed]
37. El-Atawy, M.A.; Naoum, M.M.; Al-Zahrani, S.A.; Ahmed, H.A. New Nitro-Laterally Substituted Azomethine Derivatives; Synthesis, Mesomorphic and Computational Characterizations. *Molecules* **2021**, *26*, 1927. [CrossRef] [PubMed]
38. Gomha, S.M.; Ahmed, H.A.; Shaban, M.; Abolibda, T.Z.; Alharbi, K.A.; Alalawy, H.H. New nematogenic conical-shaped supramolecular H-bonded complexes for solar energy investigations. *Sci. Rep.* **2021**, *11*, 17622.
39. Al-Mutabagani, L.A.; Alshabanah, L.A.; Ahmed, H.A.; El-Atawy, M.A. Synthesis, optical and DFT characterizations of laterally fluorinated phenyl cinnamate liquid crystal non-symmetric system. *Symmetry* **2021**, *13*, 1145. [CrossRef]
40. Khushaim, M.S.; Alalawy, H.H.; Naoum, M.M.; Ahmed, H.A. Experimental and computational simulations of nematogenic liquid crystals based on cinnamic acid in pure and mixed state. *Liq. Cryst.* **2021**, *48*, 1–12.
41. Paterson, D.A.; Abberley, J.P.; Harrison, W.T.A.; Storey, J.; Imrie, C.T. Cyanobiphenyl-based liquid crystal dimers and the twist-bend nematic phase. *Liq. Cryst.* **2017**, *44*, 127–146. [CrossRef]
42. Frisch, M.J.; Trucks, G.W.; Schlegel, H.B.; Scuseria, G.E.; Robb, M.A.; Cheeseman, J.R.; Scalmani, G.; Barone, V.; Mennucci, B.; Petersson, G.A.; et al. *Fox, Gaussian 09, Revision A.02*; Gaussian Inc.: Wallingford, CT, USA, 2009.
43. Becke, A.D. Density-functional exchange-energy approximation with correct asymptotic behavior. *Phys. Rev. A* **1988**, *38*, 3098–3100. [CrossRef] [PubMed]
44. Lee, C.; Yang, W.; Parr, R.G. Development of the Colle-Salvetti correlation-energy formula into a functional of the electron density. *Phys. Rev. B* **1988**, *37*, 785–789. [CrossRef] [PubMed]
45. Karthikeyan, M.; Glen, R.C.; Bender, A. General melting point prediction based on a diverse compound data set and artificial neural networks. *J. Chem. Inf. Model.* **2005**, *45*, 581–590. [CrossRef] [PubMed]
46. Imrie, C.T.; Taylor, L. The preparation and properties of low molar mass liquid crystals possessing lateral alkyl chains. *Liq. Cryst.* **1989**, *6*, 1–10. [CrossRef]
47. Imrie, C.T. Non-symmetric liquid crystal dimers: How to make molecules intercalate. *Liq. Cryst.* **2006**, *33*, 1449–1485.
48. Donaldson, T.; Staesche, H.B.A.F.; Lu, Z.B.; Henderson, P.A.; Achard, M.F.; Imrie, C.T. Symmetric and non-symmetric chiral liquid crystal dimers. *Liq. Cryst.* **2010**, *37*, 1097–1110.
49. Henderson, P.A.; Niemeyer, O.; Imrie, C.T. Methylene-linked liquid crystal dimers. *Liq. Cryst.* **2001**, *28*, 463–472. [CrossRef]

50. Henderson, P.A.; Imrie, C.T. Methylene-linked liquid crystal dimers and the twist-bend nematic phase. *Liq. Cryst.* **2011**, *38*, 1407–1414. [CrossRef]
51. Popoola, S.A.; Al-Harbi, M.H.M.; Al-Rashidi, A.H.; Almarwani, M.S.A.; Almohammedi, A.R.; Logunleko, A.O.; Al-Saadi, A.A. DFT evaluation of the effects of OH, NH_2 and Br substituents on the properties of 2,2′-bipyridine derivatives. *J. Taibah Univ. Sci.* **2020**, *14*, 1527–1537.
52. Popoola, S.A.; Almohammedi, A.R.; Haruna, K. Spectroscopic and DFT evaluation of the positional effect of amino group on the properties of aminobenzenesulphonic acid: Solvent interaction. *Chem. Pap.* **2021**, *75*, 2775–2789.
53. Alamro, F.S.; Ahmed, H.A.; Popoola, S.A.; Altaleb, H.A.; Al-Ola, K.A.A.; Gomha, S.M. Effect of the relative positions of di-laterally substituted schiff base derivatives: Phase transition and computational investigations. *Crystals* **2021**, *11*, 870. [CrossRef]
54. Popoola, S.A.; Onawole, A.T.; Ullah, N.; Al-Saadi, A.A. Structural and energetic effect of the intramolecular hydrogen bonding in 4,6 dihaloresorcinols: Ab initio calculation, vibrational spectroscopy, and molecular docking studies. *Struct. Chem.* **2021**, 1–13.
55. Alshabanah, L.A.; Al-Mutabagani, L.A.; Gomha, S.M.; Ahmed, H.A.; Popoola, S.A.; Shaban, M. Novel sulphonic acid liquid crystal derivatives: Experimental, computational and optoelectrical characterizations. *RSC Adv.* **2021**, *11*, 27937–27949. [CrossRef]
56. Selvarasu, C.; Kannan, P. Effect of azo and ester linkages on rod shaped Schiff base liquid crystals and their photophysical investigations. *J. Mol. Struct.* **2016**, *1125*, 234–240.
57. Alamro, F.S.; Ahmed, H.A.; El-Atawy, M.A.; Al-Zahrani, S.A.; Omar, A.Z. Induced Nematic Phase of New Synthesized Laterally Fluorinated Azo/Ester Derivatives. *Molecules* **2021**, *26*, 4546. [CrossRef]
58. McMillan, W.L. Simple molecular model for the smectic A phase of liquid crystals. *Phys. Rev. A* **1971**, *4*, 1238–1246.
59. Date, R.W.; Imrie, C.T.; Luckhurst, G.R.; Seddon, J.M. Smectogenic dimeric liquid crystals. The preparation and properties of the α, ω-bis (4-n-alkylanilinebenzylidine-4′-oxy) alkanes. *Liq. Cryst.* **1992**, *12*, 203–238. [CrossRef]